Rapid formation of uniformly layered materials by coupling reaction-diffusion processes with mechanical responsiveness

Campenhout, C.T. van; Napel, D.N. ten; Hecke, M.L. van; Noorduin, W.L.

PNAS RESEARCH ARTICLE | CHEMISTRY

Rapid formation of uniformly layered materials by coupling reaction–diffusion processes with mechanical responsiveness

Christiaan T. van Campenhout[a], Daniël N. ten Napel[a], Martin van Hecke[a,b,1], and Willem L. Noorduin[a,c,1]

Edited by Bartosz Grzybowski, Ulsan National Institute of Science and Technology, Ulsan, South Korea; received December 22, 2021; accepted August 15, 2022 by Editorial Board Member Lia Addadi

Straightforward manufacturing pathways toward large-scale, uniformly layered composites may enable the next generation of materials with advanced optical, thermal, and mechanical properties. Reaction–diffusion systems are attractive candidates to this aim, but while layered composites theoretically could spontaneously arise from reaction–diffusion, in practice randomly oriented patches separated by defects form, yielding nonuniformly patterned materials. A propagating reaction front can prevent such nonuniform patterning, as is the case for Liesegang processes, in which diffusion drives a reaction front to produce layered precipitation patterns. However, while diffusion is crucial to control patterning, it slows down transport of reactants to the front and results in a steady increase of the band spacing as the front advances. Here, we circumvent these diffusive limitations by embedding the Liesegang process in mechanically responsive hydrogels. The coupling between a moving reaction front and hydrogel contraction induces the formation of a self-regulated transport channel that ballistically carries reactants toward the area where patterning occurs. This ensures rapid and uniform patterning. Specifically, large-scale (>5-cm) uniform banding patterns are produced with tunable band distance (d = 60 to 160 μm) of silver dichromate crystals inside responsive gelatin–alginate hydrogels. The generality and applicability of our mechanoreaction–diffusion strategy are demonstrated by forming patterns of precipitates in significantly smaller microscopic banding patterns (d = 10 to 30 μm) that act as self-organized diffraction gratings. By circumventing the inherent limitations of diffusion, our strategy unlocks the potential of reaction–diffusion processes for the manufacturing of uniformly layered materials.

Liesegang patterns | periodic precipitation | reaction–diffusion | self-organization | active hydrogels

Significance

Equidistant layering of materials is central to the outstanding performance of biological minerals, such as nacre and bone, and offers exciting opportunities for classes of artificial materials with advanced functionalities. We demonstrate the self-organization of highly regular band patterns by embedding reaction–diffusion processes in mechanically responsive hydrogels. The mechanical deformation of the gel automatically regulates the local reactions conditions such that the reaction–diffusion process spontaneously generates equidistantly spaced layers. The simplicity, tunability, and generality of our self-organization strategy open exciting opportunities for exploiting reaction–diffusion processes toward fabricating components with advanced optical, mechanical, and thermal functionalities. Moreover, the here-introduced mechano-regulated chemical transport mechanism can impact our ability to understand and control pattern formation in complex and living matter.

Self-organization strategies offer powerful routes for the fabrication of the next generation of complex structured materials with advanced functionalities (1, 2). Such self-organization approaches may be particularly advantageous for the fabrication of uniformly layered materials because of their desirable mechanical, optical, and electronic properties (3–10). While such layered materials have gained tremendous attention, their manufacturing remains challenging. Therefore, simple routes toward uniformly layered materials are of fundamental interest, with practical ramifications for manufacturing approaches.

A potentially powerful self-organized manufacturing approach is offered by reaction–diffusion (RD) systems, where a delicate balance between reaction and diffusion rates induces the spontaneous formation of spatial patterns (2, 11–14). In theory, such patterns could spontaneously arrange into uniform layers (15). In practice, however, differently oriented patches separated by defects occur, and experimental inhomogeneities lead to additional deviations from uniform patterning.

In order to align patches and prevent defects, patterns can be produced with a moving reaction front, generating the pattern layer by layer in a time-ordered manner. The archetypical example of such a system is the Liesegang process (16–20). In such a system, a well-defined chemical gradient is established by placing a solution of an outer electrolyte (OE) on top of a gel matrix containing an inner electrolyte (IE) (Fig. 1*A*). The OE diffuses into the gel matrix, resulting in an OE front that moves through the gel and reacts with the IE to form an insoluble product, which precipitates at the precipitation front (x_f). This precipitate is not evenly dispersed throughout the gel matrix but rather in the form of a characteristic banding pattern, with nonuniform band spacing and bandwidth. The nonuniform patterning behavior can be explained as follows; over time, as the OE diffuses farther into the gel matrix, the diffusive zone length (g) is increased, resulting in decreasing OE concentrations at the precipitation front, causing bands to appear progressively farther apart.

The nonuniform bands produced by such Liesegang processes are undesirable for most applications. On small scales (<0.1 cm), this nonuniform behavior is less severe,

Author contributions: C.T.v.C., D.N.t.N., M.v.H., and W.L.N. designed research; C.T.v.C. and D.N.t.N. performed research; C.T.v.C., M.v.H., and W.L.N. analyzed data; and C.T.v.C., M.v.H., and W.L.N. wrote the paper.

The authors declare no competing interest.

This article is a PNAS Direct Submission. B.G. is a guest editor invited by the Editorial Board.

[1]To whom correspondence may be addressed. Email: mvhecke@gmail.com or noorduin@amolf.nl.

This article contains supporting information online at https://www.pnas.org/lookup/suppl/doi:10.1073/pnas.2123156119/-/DCSupplemental.

Published September 19, 2022.

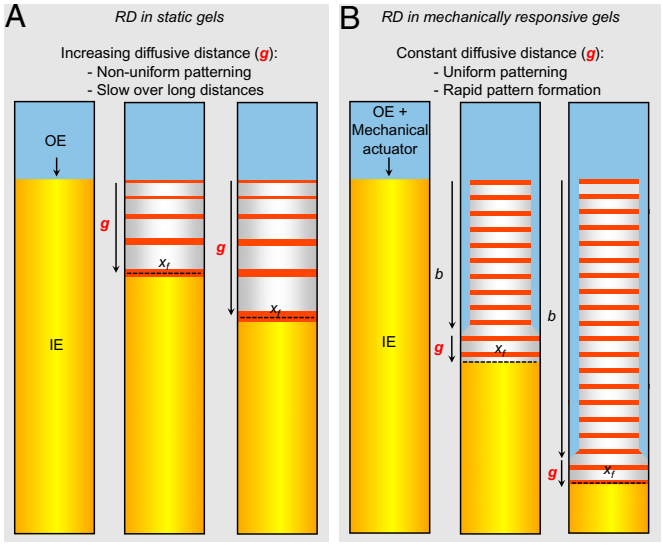

Fig. 1. Schematic representation of the here-introduced concept of RD in MRGs. (*A*) Classical Liesegang-type pattern formation. Note the increasing diffusive distance *g* and subsequent nonuniform patterning. (*B*) Pattern formation in MRGs. Note the constant diffusive distance *g* and subsequent uniform patterning.

and RD has been applied successfully for the microfabrication of optical and electronic components as well as composite-like materials (21–23). On larger scales (>0.1 cm), however, the increased diffusive zone inherently limits the practical applicability of RD processes; diffusion renders pattern formation slow and produces nonuniform layers (24). Unlocking the full potential of the Liesegang process for the self-organization of functional materials thus requires the development of a fundamentally different approach, one that overcomes the limitations inherent to diffusion while retaining the control and order of diffusion-driven pattern formation.

In this work, we present a strategy to overcome these limitations by embedding the RD process in a mechanically responsive gel (MRG) instead of a conventional static gel (SG) (Fig. 1*B*). The central idea is that contraction of the gel in response to a mechanically actuating chemical that is added to the OE induces the self-regulated formation of a transport channel that follows the precipitation front at a constant distance. This transport channel effectively divides the system into two zones: a mixing zone (*b*) and a diffusive zone (*g*). In the mixing zone, convective mixing renders chemical transport nearly instantaneous, whereas in the diffusive zone, chemical transport is diffusion limited. This combination of a constant supply of OE through a transport channel and diffusive transport at the precipitation front ensures spatiotemporally uniform and fast patterning of layered materials. In particular, the reaction front then moves ballistically (i.e., with constant speed) and not diffusively (i.e., slowing down). Hence, this strategy overcomes the inherent diffusive limitations of RD processes while retaining their desired simplicity to yield highly uniform multilayered materials with precise tunability.

Results and Discussion

To probe the mechanism where chemically induced gel contraction causes the formation of a channel, which in turn, transports reactants ballistically to the front of the channel, we develop a system where transport rates and channel formation can easily be visualized. Specifically, we follow the transport rate of the dye fluorescein in an MRG. We cast a gelatin–alginate interpenetrating network (GA-IPN) in a cylindrical tube and place a solution (10 mL) of fluorescein (1.5 mM) and the mechanical actuator calcium nitrate (2.4 M) on top; calcium ions shrink the gel by cross-linking alginate (Fig. 2*A*) (25). Consistent with our proposed scenario, in MRGs a clearly visible channel (a gap between the gel and tube) opens, directly connecting the OE reservoir with the reaction zone (Fig. 2*B*). In contrast to the diffusive transport observed in SGs, in MRGs we observe that the rate of transport is constant over time, indicative of ballistic transport (Fig. 2*C*). Moreover, in an SG, chemical transport over 4 cm takes over 99.4 h, whereas in MRGs, this same distance is reached more than 10 times faster in merely 8.4 h, showing that MRGs allow for rapid transport over long distances.

To explicitly show that channel formation induces flow through the channel from the dye reservoir toward the transport front, we monitor the experiment with Schlieren microscopy. This optical technique visualizes flow by revealing differences in refractive index and thus differences in density. Using this technique, we observe convective flow only in the presence of the gap (Movie S1). Additionally, closer inspection of the transport front shows that gap formation is preceded by a diffusive zone with a constant length (*g*) (Fig. 2*B*). Channel formation in MRGs thus induces ballistic transport toward a diffusion zone of constant width.

The constant transport rate in MRGs suggests that different, and perhaps uniform, types of pattern formation may be achieved

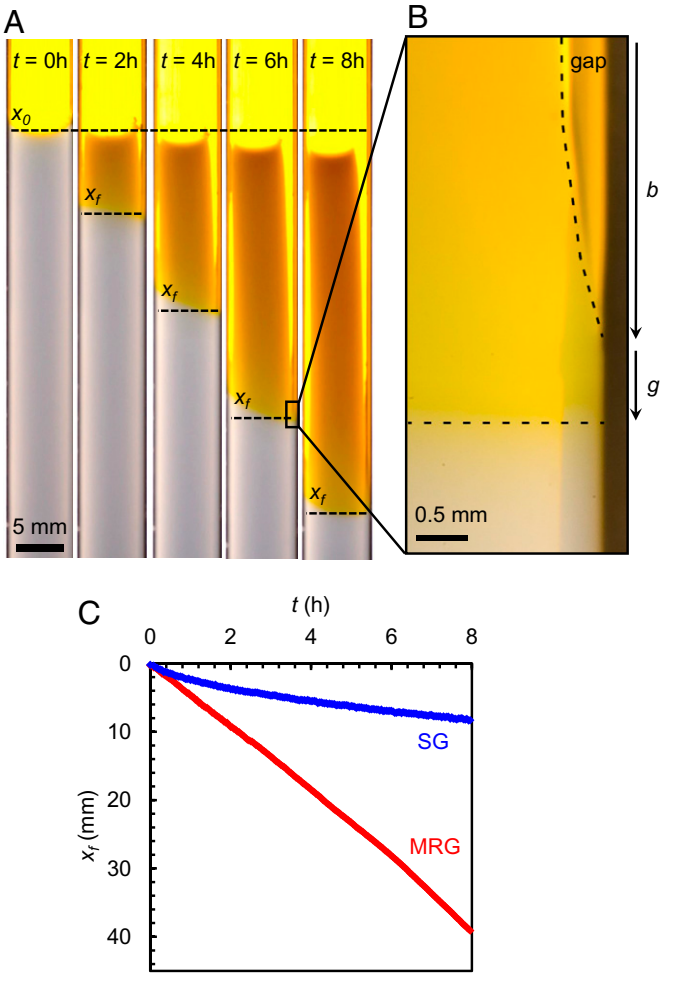

Fig. 2. (*A*) Time-lapse series showing the transport of fluorescein in an MRG. (*B*) Close-up photograph of an MRG showing the formation of a channel that enables ballistic transport toward the front. (*C*) x_f–*t* plot showing slow diffusive transport in SG (blue line) and rapid ballistic transport in MRG (red line).

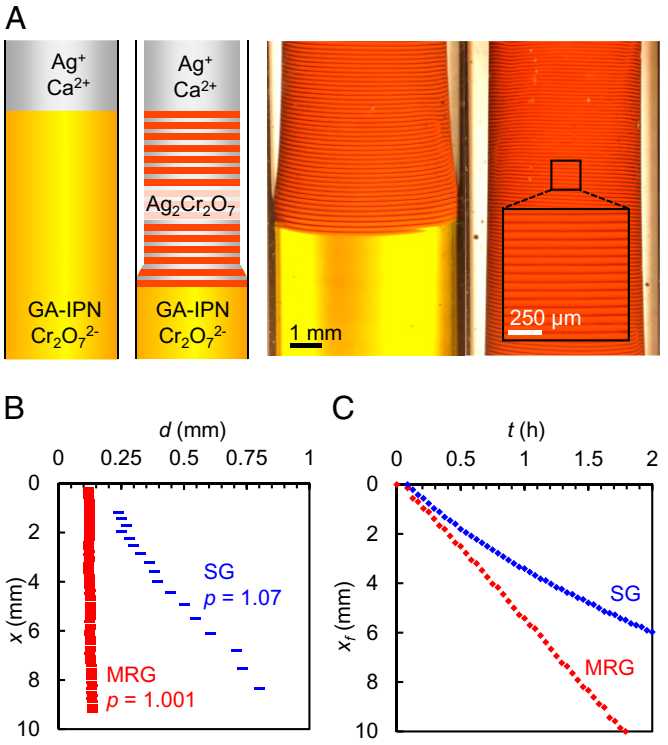

Fig. 3. Periodic precipitation in an MRG. (*A*) Equidistant pattern formation of $Ag_2Cr_2O_7$ in a GA-IPN. (*B*) The band distance increases for SG ($p = 1.07 \pm 0.03$) and remains constant for MRG ($d = 120$ µm, $p = 1.001 \pm 0.002$). (*C*) The *x*–*t* plot shows diffusive precipitation in SG (blue line) and rapid ballistic transport in MRG (red line). Note that the curved appearance of the banding pattern is an optical effect caused by the cylindrical shape of the gel and its container. Cross-sectioning of a gel reveals a flat, noncurved pattern (*SI Appendix*, Fig. S3).

by coupling traditional RD processes with MRGs. To exploit this potential, we embed Liesegang periodic precipitation in an MRG. We allow a combination of OE (0.8 M $AgNO_3$) and a mechanical actuator [2.4 M $Ca(NO_3)_2$] to diffuse into a GA-IPN containing the IE (17 mM $K_2Cr_2O_7$), which reacts to form a precipitation pattern of $Ag_2Cr_2O_7$ (Fig. 3*A*; Movie S2 shows a time-lapse of this pattern forming, and *SI Appendix*, Fig. S1 shows a larger-scale image). We note that in this example, we use large volumes of OE (20 mL) compared with the total gel volume (1.5 mL). This is because we want to limit the effect of concentration losses in the OE due to dilution and consumption by precipitation. We have investigated the effects of such concentration losses on patterning behavior and found that for sufficiently large yet realistic volumes of OE, these effects are negligible (*SI Appendix*, Fig. S2). Indeed, for the experiment performed here, the patterns appear equidistant under visual inspection (Fig. 3 *A* and *B*).

To quantify the equidistant nature of the pattern, we follow the standard approach where we define the spacing fraction as the fraction of subsequent band locations, $p_n := \frac{x_{n+1}}{x_n}$, and then determine $p := \lim_{n\to\infty} p_n$. In SGs, $p > 1$ is observed, which corresponds to a banding pattern where the distance between subsequent bands (d) increases over time. In contrast, in MRGs, we observe highly regular equidistantly spaced periodic precipitation with a constant band distance ($d = 126 \pm 4.6$ µm) (Fig. 3*B*) and uniform bandwidth ($w = 67 \pm 4.6$ µm). For large n, p_n tends to converge to its asymptotic value as $1/n$; hence, a very accurate determination for p, as well as its error bar, is obtained by plotting p_n as function or $1/n$ and extrapolating the data to $n \to \infty$ (*SI Appendix* has a detailed explanation of determining the band spacing and bandwidth and of estimating p; *SI Appendix*, Figs. S1 and S3). For our MRG, we find that $p = 1.001 \pm 0.002$; hence, for large n and x, our pattern is equidistant within our error bar, confirming the visual observation of constant band spacing (Fig. 3*B* and *SI Appendix*, Fig. S4). Simultaneously, a clearly visible channel is formed, which closely follows the precipitation front that propagates at a constant and high rate (5 mm/h) (Fig. 3*C*). Hence, MRGs allow periodic precipitation reactions to rapidly form asymptotically equidistant patterns.

To further verify our channel formation–ballistic transport scenario and to quantitatively understand the role of the additional parameters introduced, we develop a numerical model. Inspired by previous RD models, we compute the reaction of the IE and OE using first- and second-order reaction kinetics (*Materials and Methods* and Movie S3). To describe MRGs, we model the mechanical response via second-order reactivity between calcium and alginate and assume that a transport channel opens once this reaction exceeds a specified threshold, allowing ballistic transport of the OE (Fig. 4). As expected, modeling of periodic precipitation in SGs shows diffusive transport and subsequently, nonequidistant Liesegang patterns (Fig. 4 *A*, *C*, and *D*), whereas modeling of periodic precipitation in MRGs shows ballistic transport and equidistant patterning (Fig. 4 *B*–*D*).

Our model allows for efficient screening of the increased parameter space of RD processes in MRGs and directly assesses its effect on patterning behavior. Crucially, our model shows that increasing the calcium concentration speeds up the front rate v (Fig. 5*A*) and lowers the band distance d (Fig. 5*B*). We propose that this is caused by the following mechanism; at higher calcium concentrations, the shrinkage rate increases and leads to a shorter diffusive zone (Fig. 5*C*), which at the precipitation front, causes a higher OE concentration, in turn resulting in shorter band

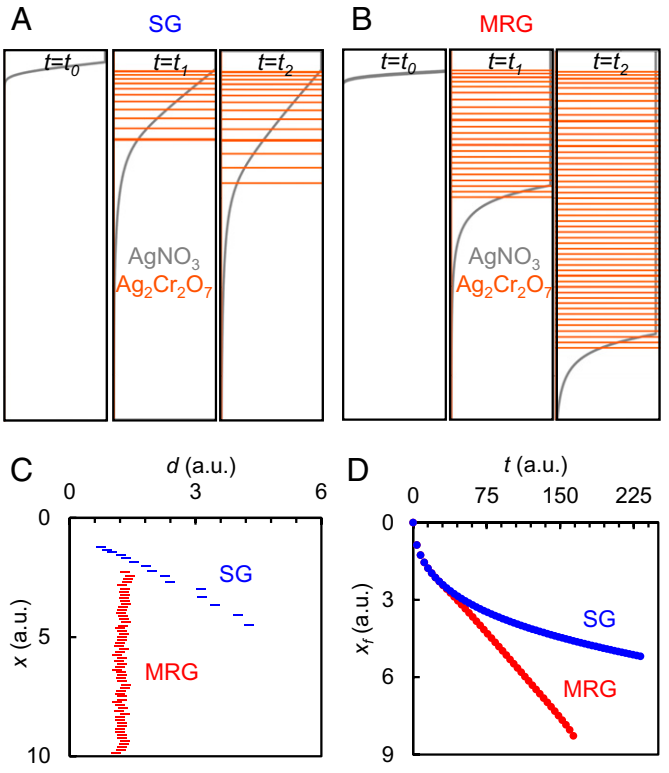

Fig. 4. Numerical modeling accurately reproduces uniform pattern formation in MRGs. Modeling of periodic precipitation shows (*A*) Liesegang patterns in a SG and (*B*) uniform patterning in an MRG. (*C*) Modeling reproduces different p values found in SGs and MRGs. (*D*) Modeling confirms diffusive transport observed in SGs and ballistic transport observed in MRGs. Note that all modeled units are arbitrary units (a.u.).

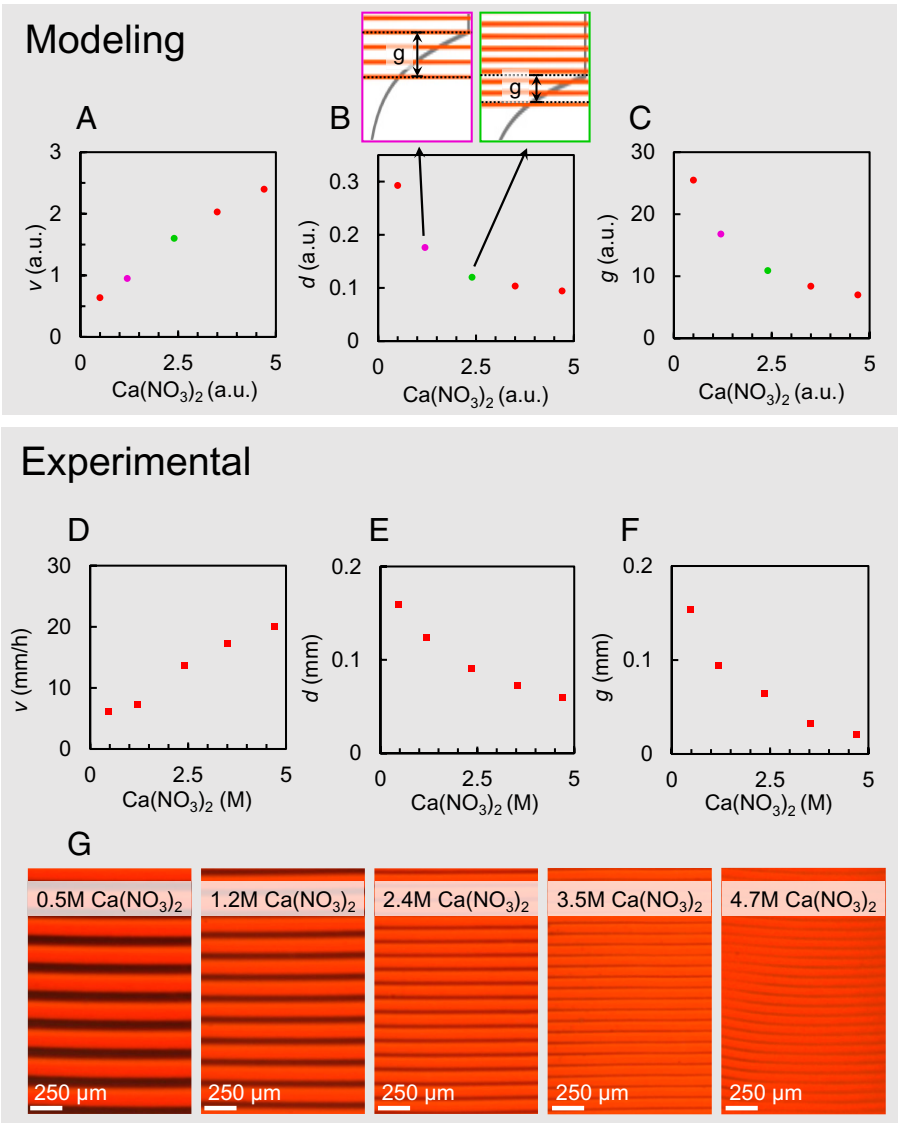

Fig. 5. Model-guided tunability of periodic precipitation in MRG. (*A*) Modeled relation between the $Ca(NO_3)_2$ concentration and transport rate (v). (*B*) The model predicts that the band distance decreases for increasing $Ca(NO_3)_2$ concentrations. (*C*) The model predicts a decreased diffusive zone (g) for higher $Ca(NO_3)_2$ concentrations. (*D–F*) Experimental relation between $Ca(NO_3)_2$ concentration and (*D*) transport rate (v), (*E*) band distance (d), or (*F*) diffusive zone length (g). (*G*) Experimental tuning of the precipitation pattern by modulation of the $Ca(NO_3)_2$ concentration. Note that all modeled units are arbitrary units (a.u.).

distances. Guided by these modeling insights, we explore how the band distance in MRGs can be controlled by modulating the calcium ion concentration in the reservoir solution. Consistent with modeling, we observe that higher calcium concentrations indeed result in shorter diffusive zone lengths (Fig. 5*D*) and subsequently, shorter band distances (Fig. 5*E*) as well as increased transport rates (Fig. 5*F*). We find that varying the concentration of calcium between 0.47 and 4.7 M enables tuning of the band distance between $d = 160$ µm and $d = 60$ µm, respectively (Fig. 5*G*). Hence, coupling of MRGs with periodic precipitation reactions enables equidistant patterns with unique mechanical-mediated tunability.

Our strategy of enhancing periodic pattern formation processes via ballistic transport in MRGs can readily be extended to other pattern formation processes employing responsive gels. This versatility and tunability opens exciting opportunities for fabricating functional self-organized periodic composites. We explore this potential by embedding an RD system that yields patterned silver nanocrystals into our MRGs to form a self-organized optical diffraction grating (Fig. 6*A*) (26). To this aim, we infiltrate a gelatin–alginate MRG containing NH_4OH (5.9 µM) with a solution of $AgNO_3$ (0.8 M) and $Ca(NO_3)_2$ (0.5 to 2.4 M) (Fig. 6*B*), inducing tunable precipitation of equidistant, narrowly spaced bands ($d = 15$ to 30 µm) of silver nanoparticles (150 to 200 nm in diameter) (Fig. 6*C*). Irradiating the periodic composite with a green laser ($\lambda = 532$ nm) shows a diffraction pattern that is in good agreement with the band spacing of the silver nanoparticles [$d = \frac{m\lambda}{2sin(\theta)}$; calculated: $d = 25.2$ µm; observed: $d = 25.8$ µm] (Fig. 6*D*), illustrating potential for self-organized functional materials.

Conclusion

In summary, we introduce here a versatile strategy to overcome diffusive limitations of the Liesegang process by exploiting mechanically responsive hydrogels. We show that the self-regulated formation of a transport channel ballistically carries reactants toward an RD zone, where diffusion-controlled pattern formation occurs. This combination of long-range ballistic transport and short-range diffusive control allows rapid formation of uniform patterns. Furthermore, we demonstrate straightforward pattern tunability and show that our strategy can readily be applied to

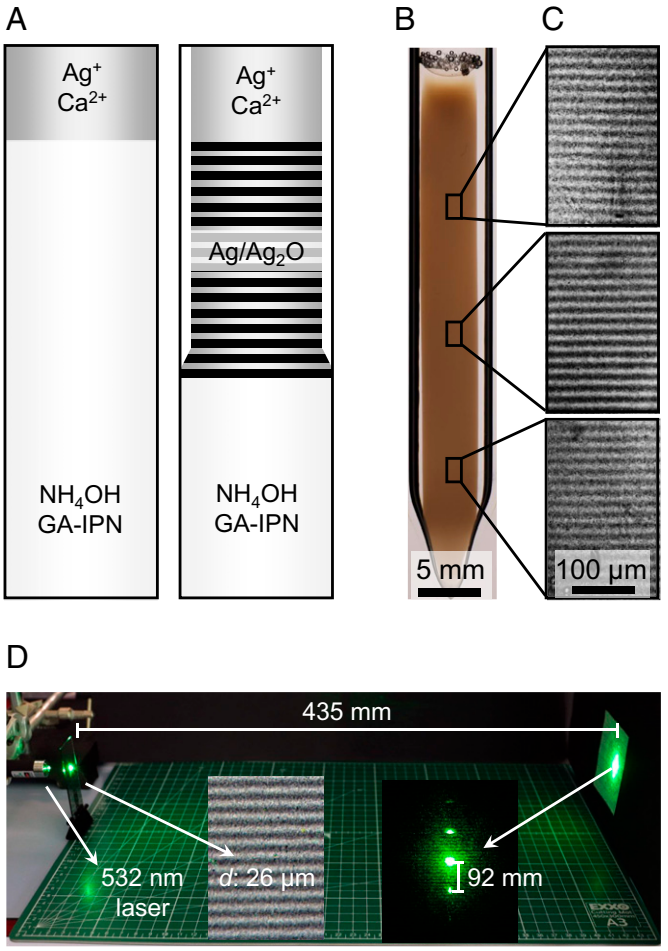

Fig. 6. Generality, scalability, and functionality potential of mechanically coupled periodic precipitation. (*A*) Schematic representation of the experimental setup used. (*B*) Macroscopic image of a GA-IPN MRG containig a microscopic pattern of silver nanoparticles. (*C*) A cross-section of the MRG reveals the equidistant microscopic banding pattern ($d = 17$ µm). (*D*) Irradiation of a different microscopic pattern ($d = 26$ µm) with a green laser (532 nm) yields diffractive patterns.

other RD systems. Although our method is limited by the compatibility of the mechanically responsive materials, their actuators, and the RD systems, we believe that, as more and more responsive materials are developed for applications such as drug delivery and sensing, exciting opportunities will arise (25). Collectively, by circumventing the inherent limitations of diffusion, our strategy unlocks the full potential of RD processes for the manufacturing of high-performance, uniformly layered materials.

As chemical transport plays essential roles in artificial and natural processes, we envisage that using mechanically active materials to bypass diffusion limitations will enhance our understanding of and control over chemical transport in complex artificial and living matter (27). Additionally, we foresee that embedding RD processes in mechanically responsive metamaterials offers a general strategy to realize complex self-organized materials that are otherwise difficult to make (28). Finally, we envisage that embedding RD processes in mechanically responsive metamaterials will lead to exciting opportunities for the generation of complex patterns with advanced functionalities.

Materials and Methods

All chemicals were used without additional purification. Gelatin was purchased from Sigma-Aldrich and was type A from porcine skin (roughly 300 g Bloom). Sodium alginate was purchased from PanReac AppliChem and was of medium viscosity (350 to 550 mPa·s at 1%), with a molecular weight of 10,000 to 600,000 g/mol.

Rate Analysis. In order to analyze precipitation rates, time lapses were made of all samples. To prevent imaging complications caused by the curvature of the used glass cylinders, all samples were placed in a custom-built glass container with immersion oil. These time lapses were analyzed using a Python3 script, which follows the position of the precipitation front over time.

Fluorescein Dye Experiments. In a typical experiment, 50 g of gel stock was prepared by dissolving gelatin (2.5 g, 5 wt %) in hot water (47.5 mL, 65 °C). Aliquots (roughly 1.2 mL) of this hot solution were then transferred to cylindrical glass tubes (60 × 0.6 mm) and allowed to cool down to room temperature (RT) by which the gels had solidified. The mechanically responsive counterparts were produced by simply dissolving sodium alginate (0.25 g, 0.5 wt %) in water prior to the addition of gelatin.

The experiment was started by mounting a syringe (10 mL) without a stopper onto these glass tubes that was subsequently filled with 10 mL of either just fluorescein (1.5 mM) for SGs or a combination of fluorescein (1.5 mM) and $Ca(NO_3)_2$ (2.4 M) for MRGs.

Potassium Dichromate Gel Preparation. In a typical experiment, 50 g of gel stock was prepared by dissolving gelatin (2.5 g, 5 wt %) in hot water (47.5 mL, 65 °C) and adding $K_2Cr_2O_7$ (250 mg). Aliquots (roughly 1.5 mL) of this hot solution were then transferred to cylindrical glass tubes (60 × 0.6 mm) and allowed to cool down to RT, by which the gels had solidified. The mechanically responsive counterparts were produced by simply dissolving sodium alginate (0.25 g, 0.5 wt %) in water prior to the addition of gelatin.

Precipitation was induced by mounting a syringe without a stopper onto these glass tubes that was subsequently filled with 20 mL of either $AgNO_3$ (0.2 to 0.8 M) for SGs or a combination of $AgNO_3$ (0.2 to 0.8 M) and $Ca(NO_3)_2$ (0.5 to 4.9 M) for MRGs.

Ammonia Gel Preparation. In a typical experiment, 50 g of gel stock was prepared by dissolving gelatin (2.5 g, 5 wt %) in hot water (47.5 mL, 65 °C) and adding NH_4OH (25%, 22 µL). Aliquots (roughly 1.5 mL) of this hot solution were then transferred to cylindrical glass tubes (60 × 0.6 mm) and allowed to cool down to RT, by which the gels had solidified. The mechanically responsive counterparts were produced by simply dissolving sodium alginate (0.25 g, 0.5 wt %) in water prior to the addition of gelatin. Precipitation was induced by mounting a syringe without a stopper onto these glass tubes that was subsequently filled with 20 mL of either $AgNO_3$ (0.2 to 0.8 M) for SGs or a combination of $AgNO_3$ (0.2 to 0.8 M) and $Ca(NO_3)_2$ (0.5 to 4.9 M) for MRGs. After precipitation in the entire gel column was complete, gels were cut into thin slices. These slices were analyzed under a Leica DMRX microscope (*SI Appendix*, Fig. S5).

Schlieren Imaging. Schlieren imaging highlights differences in density and is used to visualize flow. High turbulence indicates convective flow, whereas static areas indicate diffusion-limited regions. Since the curved surface of the typically used containers prevented effective Schlieren microscopy, different samples were prepared. Instead of cylindrical glass tubes, an MRG was now cast in between two glass microscopy slides separated by a rubber spacer (1 mm), which allowed us to observe a flat surface. The aforementioned transport channel now forms in between these glass slides and the hydrogel surface. The result of this measurements can be seen in Movie S1.

Elasto-RD Model. The RD system modeled here is the periodic precipitation of silver dichromate in a gelatin hydrogel as a result of silver nitrate diffusing into the gel matrix and reacting with potassium dichromate to produce an insoluble salt (Eq. **1**):

$$2Ag^+(aq) + Cr_2O_7{}^{2-}(aq) \rightarrow Ag_2Cr_2O_7(s). \quad \textbf{[1]}$$

In this prenucleation model, this reaction is split into three steps: 1) sol formation, 2) nucleation, and 3) growth.

1) First, a sol of $Ag_2Cr_2O_7$ is formed (Eq. **2**):

$$2Ag^+(aq) + Cr_2O_7{}^{2-}(aq) \underset{k_1}{\longrightarrow} Ag_2Cr_2O_7(aq). \quad \textbf{[2]}$$

2) This sol only nucleates after a specified nucleation threshold c^* is exceeded (Eq. **3**):

$$Ag_2Cr_2O_7(aq) \underset{k2}{\longrightarrow} Ag_2Cr_2O_7(s). \quad \textbf{[3]}$$

3) Growth onto these nuclei is autocatalytic and extremely rapid (Eq. **4**):

$$Ag_2Cr_2O_7(aq) + Ag_2Cr_2O_7(s) \underset{k3}{\longrightarrow} 2Ag_2Cr_2O_7(s). \quad \textbf{[4]}$$

These reactions form the basis for a set of RD equations, where we assume a one-dimensional geometry (Eqs. **5–8**):

$$\frac{\partial[Ag^+]}{\partial t} = D\frac{\partial t}{\partial x^2}[Ag^+] - 2k_1[Ag^+][{Cr_2O_7}^{2-}], \quad \textbf{[5]}$$

$$\frac{\partial[{Cr_2O_7}^{2-}]}{\partial t} = D\frac{\partial t}{\partial x^2}[{Cr_2O_7}^{2-}] - 2k_1[Ag^+][{Cr_2O_7}^{2-}], \quad \textbf{[6]}$$

$$\begin{aligned}\frac{\partial[Ag_2Cr_2O_7]_{aq}}{\partial t} &= D\frac{\partial t}{\partial x^2}[Ag_2Cr_2O_7]_{aq} + 2k_1[Ag^+][{Cr_2O_7}^{2-}] \\ &\quad - k_2[Ag_2Cr_2O_7]_{aq}\theta([Ag_2Cr_2O_7]_{aq} - c^*) \\ &\quad - k_3[Ag_2Cr_2O_7]_{aq}[Ag_2Cr_2O_7]_s, \end{aligned} \quad \textbf{[7]}$$

$$\begin{aligned}\frac{\partial[Ag_2Cr_2O_7]_s}{\partial t} &= k_2[Ag_2Cr_2O_7]_{aq}\theta([Ag_2Cr_2O_7]_{aq} - c^*) \\ &\quad + k_3[Ag_2Cr_2O_7]_{aq}[Ag_2Cr_2O_7]_s. \end{aligned} \quad \textbf{[8]}$$

We have verified that this set of RD equations describes Liesegang-like, diffusion-limited pattern formation (Fig. 4 *A*, *C*, and *D*).

In MRGs, we introduce gel shrinkage by adding calcium ions to the OE mixture and alginate strands to the gel. To include this in the model, we compute the cross-linking of alginate (A^-) by $Ca2^+$ to yield a Ca–alginate ($Ca - 2A$) complex (Eq. **9**):

$$Ca^{2+} + 2A^- \underset{k5}{\overset{k4}{\rightleftharpoons}} Ca - 2A. \quad \textbf{[9]}$$

The loss of free Ca^{2+} ions caused by this is given by a second-order rate equation. Since this coordination is an equilibrium reaction, we also include the opposite decoordination. This gives the following RD equations for $[Ca^{2+}]$, $[A^-]$, and $[Ca - 2A]$ (Eqs. **10–12**):

$$\frac{\partial[Ca^{2+}]}{\partial t} = D\frac{\partial t}{\partial x^2}[Ca^{2+}] - k_4[Ca^{2+}][A^-]^2 + k_5[Ca - 2A], \quad \textbf{[10]}$$

$$\frac{\partial[A^-]}{\partial t} = -2k_4[Ca^{2+}][A^-]^2 + 2k_5[Ca - 2A], \quad \textbf{[11]}$$

$$\frac{\partial[Ca - 2A]}{\partial t} = k_4[Ca^{2+}][A^-]^2 - k_5[Ca - 2A]. \quad \textbf{[12]}$$

To add channel formation, we first define the leading edge of channel formation, x_e, as the final instance where $[Ca - 2A]$ exceeds a specified threshold a^*. For $x < x_e$, chemical transport is instantaneous, and solutes are evenly distributed, whereas for $x > x_e$, chemical transport is diffusion limited. To compensate for dilution effects, we have introduced V_{in} and V_{out}, the volumes of IE and OE used, respectively. This results in the following equation for solute concentrations where $x < x_e$ (Eq. **13**) (X = any solute):

$$\begin{aligned}[X]_{channel} &= [X]_0\frac{V_{out}}{V_{out} + \beta V_{in}} \\ with\ \beta &= \frac{l_{channel}}{l_{system}}. \end{aligned} \quad \textbf{[13]}$$

Here, the concentration of solute in the channel $[X]_{channel}$ is calculated from its starting concentration $[X]_0$, the starting volumes used V_{in} and V_{out}, and β, which uses the length of the channel and the length of the entire system to describe the relative distance the channel has opened (returns zero at t_0 and one at t_∞). Introducing the aforementioned periodic precipitation reactions (Eqs. **5–8**) into this MRG model accurately reproduces experimentally observed transport rates as well as equidistant patterning behavior (Fig. 4 *B–D*).

Data, Materials, and Software Availability. All study data are included in the article and/or supporting information.

ACKNOWLEDGMENTS. We thank Hinco Schoenmaker for technical support. This research received funding from the Dutch Research Council in the framework of the ENW PPP Fund for the top sectors and from the Ministry of Economic Affairs in the framework of the PPS-Toeslagregeling.

Author affiliations: [a]AMOLF, Amsterdam 1098 XG, the Netherlands; [b]Leiden Institute of Physics, Leiden University, Leiden 2333 CA, the Netherlands; and [c]Van 't Hoff Institute for Molecular Sciences, University of Amsterdam, Amsterdam 1090 GD, the Netherlands

1. G. M. Whitesides, B. Grzybowski, Self-assembly at all scales. *Science* **295**, 2418–2421 (2002).
2. L. Cera, C. A. Schalley, Under diffusion control: From structuring matter to directional motion. *Adv. Mater.* **30**, e1707029 (2018).
3. R. M. Parker *et al.*, The self-assembly of cellulose nanocrystals: Hierarchical design of visual appearance. *Adv. Mater.* **30**, e1704477 (2018).
4. A. Finnemore *et al.*, Biomimetic layer-by-layer assembly of artificial nacre. *Nat. Commun.* **3**, 966 (2012).
5. L. B. Mao *et al.*, Synthetic nacre by predesigned matrix-directed mineralization. *Science* **354**, 107–110 (2016).
6. A. McDougal, B. Miller, M. Singh, M. Kolle, Biological growth and synthetic fabrication of structurally colored materials. *J. Opt.* **21**, 073001 (2019).
7. M. Eder, S. Amini, P. Fratzl, Biological composites-complex structures for functional diversity. *Science* **362**, 543–547 (2018).
8. A. R. Studart, Towards high-performance bioinspired composites. *Adv. Mater.* **24**, 5024–5044 (2012).
9. S. Deville, E. Saiz, R. K. Nalla, A. P. Tomsia, Freezing as a path to build complex composites. *Science* **311**, 515–518 (2006).
10. M. V. Dinu, M. M. Ozmen, E. S. Dragan, O. Okay, Freezing as a path to build macroporous structures: Superfast responsive polyacrylamide hydrogels. *Polymer (Guildf.)* **48**, 195–204 (2007).
11. Z. Tan, S. Chen, X. Peng, L. Zhang, C. Gao, Polyamide membranes with nanoscale Turing structures for water purification. *Science* **360**, 518–521 (2018).
12. S. Kondo, T. Miura, Reaction-diffusion model as a framework for understanding biological pattern formation. *Science* **329**, 1616–1620 (2010).
13. J. Horváth, I. Szalai, P. De Kepper, An experimental design method leading to chemical Turing patterns. *Science* **324**, 772–775 (2009).
14. A. M. Turing, The chemical basis of morphogenesis. *Philos. Trans. R. Soc. London Ser. B Biol. Sci* **237**, 37–72 (1952).
15. M. C. Cross, P. C. Hohenberg, Pattern formation outside of equilibrium. *Rev. Mod. Phys.* **65**, 851 (1993).
16. R. E. Liesegang, Uber einige eigenschaften von gallerten. *Naturwissensch Wochenschr* **11**, 353–362 (1896).
17. A. J. Ackroyd *et al.*, Self-organization of nanoparticles and molecules in periodic Liesegang-type structures. *Sci. Adv.* **7**, 3801–3817 (2021).
18. H. Nabika, M. Itatani, I. Lagzi, Pattern formation in precipitation reactions: The Liesegang phenomenon. *Langmuir* **36**, 481–497 (2020).
19. E. Nakouzi, O. Steinbock, Self-organization in precipitation reactions far from the equilibrium. *Sci. Adv.* **2**, e1601144 (2016).
20. O. Giraldo *et al.*, Spontaneous formation of inorganic helices. *Nature* **405**, 38 (2000).
21. C. J. Campbell *et al.*, Self-organization of planar microlenses by periodic precipitation. *J. Appl. Phys.* **97**, 126102 (2005).
22. S. K. Smoukov, A. Bitner, C. J. Campbell, K. Kandere-Grzybowska, B. A. Grzybowski, Nano- and microscopic surface wrinkles of linearly increasing heights prepared by periodic precipitation. *J. Am. Chem. Soc.* **127**, 17803–17807 (2005).
23. B. A. Grzybowski, K. J. Bishop, C. J. Campbell, M. Fialkowski, S. K. Smoukov, Micro- and nanotechnology via reaction-diffusion. *Soft Matter* **1**, 114–128 (2005).
24. B. A. Grzybowski, *Chemistry in Motion: Reaction-Diffusion Systems for Micro- and Nanotechnology* (John Wiley & Sons, 2009).
25. Y. Dong, A. N. Ramey-Ward, K. Salaita, Programmable mechanically active hydrogel-based materials. *Adv. Mater.* **33**, e2006600 (2021).
26. R. M. Walliser *et al.*, Understanding the formation of aligned, linear arrays of ag nanoparticles. *RSC Advances* **6**, 28388–28392 (2016).
27. Y. Li, K. Konstantopoulos, R. Zhao, Y. Mori, S. X. Sun, The importance of water and hydraulic pressure in cell dynamics. *J. Cell Sci.* **133**, jcs240341 (2020).
28. M. Kadic, G. W. Milton, M. van Hecke, M. Wegener, 3D metamaterials. *Nat. Rev. Phys* **1**, 198–210 (2019).